Available online at www.sciencedirect.com
SCIENCE DIRECT®
Pergamon
Acta Materialia 51 (2003) 17–30
Acta MATERIALIA
www.actamat-journals.com

Phase field methods and dislocations

D. Rodney, Y. Le Bouar, A. Finel *

Laboratoire d'Etude des Microstructures, CNRS-ONERA, B.P. 72, 92322 Châtillon Cedex, France

Received 20 July 2001; accepted 8 September 2001

Abstract

We present a general formalism for incorporating dislocations in Phase Field methods (PFM) based on the elastic equivalence between a dislocation loop and a platelet inclusion of specific stress-free strain. Dislocations may be elastically and dynamically coupled to any other field such as a concentration field. Special attention is paid to the treatment of dislocation cores after the discretization of real and reciprocal space required by the computer implementation of any PFM. In particular, we propose a method based on two length scales to account for dislocation cores much smaller than the grid spacing. The method is illustrated through the simulation of the motion of a dislocation loop in a microstructure representative of a late-stage γ/γ' microstructure.

Keywords: Dislocations; Phase field; Microstructure; Micronscale; Elasticity

1. Introduction

The elaboration and design of alloys involves the mutual interactions between dislocations and alloying elements. Dislocations are well known to be preferential sites for the segregation of solute atoms (Cottrell atmospheres [1]) as well as for the nucleation of precipitates (heterogeneous precipitation [2]). Inversely, solute atmospheres and precipitates are obstacles to dislocation motion and are at the origin of structural hardening [3].

Phase transformations and dislocations can be simulated at the micronscale. On the one hand, Phase Field methods (PFM) are powerful tools to study microstructural evolutions during phase transformations [4,5]. On the other hand, the dynamics of three-dimensional (3D) dislocation microstructures may be simulated at the micronscale using Discrete Dislocation Dynamics (DDD) [6,7].

Up to now, the coupling between dislocations and phase transformations has rarely been addressed in the context of micronscale simulations. The presence of misfitting inclusions in DDD simulations has been accounted for only by means of a background coherency stress, not evolving with time [6]. The first attempt to introduce dislocations in a PFM is due to Léonard and Desai [8] who studied the influence of dislocations on spinodal decomposition. Their model is, however, limited to static edge or screw dislocations in a two-dimensional (2D) elastically isotropic medium. Hu and Chen [9] used Mura's theory of eigenstrains

* Corresponding author. Tel.: +33-1-4673-4452; fax: +33-1-4673-4155.
E-mail address: alphonse.finel@onera.fr (A. Finel).

1359-6454/03/$22.00
doi:10.1016/S1359-6454(01)00379-2

[10] to introduce dislocations in a PFM and study solute segregation and nucleation of coherent particles around 2D static edge dislocations.

Recently, a new Phase Field approach, which allows for the application of dynamics to the dislocations, has been proposed [11,12]. It is based on an analogy first pointed out by Nabarro [13] between a dislocation loop and a platelet inclusion. Any planar dislocation loop may be modeled elastically as a platelet inclusion, bordered by the dislocation loop, with a stress-free strain related to the Burgers vector **b** and normal **n** of the loop by $\epsilon_{ij}^{00} = (b_i n_j + b_j n_i)/2a$, where a is the interplanar distance. This analogy was used by Wang, Jin, Cuitiño and Khachaturyan [11] and by Rodney and Finel [12] to introduce dislocations in a PFM as extra phases. These authors used a Diffuse Interface approach to apply dynamics on the dislocation fields. However, as shown below, this approach leads to very wide cores not compatible with experimental cores. Since the core radius controls the maximum stress near dislocations and thus the short range interactions between dislocations and between dislocations and concentration fields, a new scheme was needed.

In this article, we present an improved version of this Phase Field method which accounts for angström-scale dislocation cores in a micronscale simulation cell while keeping the generality of the initial method: it is valid for any 3D anisotropic elastic medium with any dislocation distribution and couples dynamically the dislocations to any other field such as a concentration field.

We will focus here mainly on the characteristics of the method. Its applications to the study of plasticity in alloys will be addressed in a future publication. The paper is organized as follows. In Section 2, we present the method to model dislocations as extra phases in a PFM. In Section 3, we consider the implications of the discretization of real space required by the computer implementation of any PFM on the dislocation core size and propose a method to account for dislocation cores smaller than the grid spacing. In Section 4, we present dynamical equations for the dislocations compatible with narrow cores. In Section 5, we present a diffusion model for a concentration field which can be used in the presence of dislocations. In Section 6, the method is applied to the simulation of a dislocation gliding in a complex microstructure. Finally, in Section 7, we summarize our results and conclude.

2. Static method in a continuous medium

We present here the method to incorporate static dislocations in a PFM. In this section, we focus on a continuous medium while in the next section, we will consider a discretized medium as is the case in practice, when the PFM is implemented in a computer.

2.1. Phase field microelasticity theory

The present model is based on the Phase Field Microelasticity theory developed by Khachaturyan [14]. This theory is briefly summarized here in order to recall its basic assumptions and to clarify our notations.

We consider a homogeneous elastic medium with elastic tensor λ_{ijkl}, subjected to an external uniform stress σ_{ij}^{A}. The system is composed of several phases, noted p, which are each characterized by their shape function $\theta_p(\mathbf{r})$ (equal to 1 or 0 whether the system at point **r** is in phase p or not) and their stress-free strain $\epsilon_{ij}^{00}(p)$. The local stress-free strain is the sum of the stress-free strains of the various phases:

$$\epsilon_{ij}^{0}(\mathbf{r}) = \sum_{p:phase} \epsilon_{ij}^{00}(p)\theta_p(\mathbf{r}) \tag{1}$$

The elastic energy in a system of volume V is:

$$E^{el} = \frac{1}{2}\int_V dV\, \lambda_{ijkl}(\epsilon_{ij}(\mathbf{r}) - \epsilon_{ij}^{0}(\mathbf{r}))(\epsilon_{kl}(\mathbf{r}) - \epsilon_{kl}^{0}(\mathbf{r})) \tag{2}$$

$$- \int_V dV\, \sigma_{ij}^{A}\epsilon_{ij}(\mathbf{r})$$

The equilibrium state of the system is obtained analytically in reciprocal space, by decomposing the strain field $\epsilon_{ij}(\mathbf{r})$ into homogeneous and inhomogeneous strain fields and imposing periodic boundary conditions to the inhomogeneous strain

field. The following definitions for the Fourier transforms are used:

$$\theta(\mathbf{K}) = \frac{1}{V}\int_V dV\,\theta(\mathbf{r})\mathrm{e}^{-i\mathbf{K}\mathbf{r}}$$
$$\theta(\mathbf{r}) = \sum_K \theta(\mathbf{K})\mathrm{e}^{i\mathbf{K}\mathbf{r}} \tag{3}$$

The backward Fourier transform is a sum over discrete K-vectors $\left(K_\mathrm{i} = 2\pi\frac{n_\mathrm{i}}{L_\mathrm{i}}\right)$ because of the periodic boundary conditions. This sum is unbounded in a continuous medium, i.e. $n_\mathrm{i} \in \mathbb{Z}$. Note that, in a discretized medium, as is the case in any computer implementation, K-vectors are limited to the first Brillouin zone of the grid ($-\pi/d < \mathrm{K_i} \leq \pi/d$, where d is the grid spacing).

The condition of elastic equilibrium yields displacements:

$$u_\mathrm{i}(\mathbf{r}) = \sum_{\mathbf{K}\neq 0}\sum_{p:phase} -iG_\mathrm{im}(\mathbf{K})\sigma^0_\mathrm{mn}(p)\theta_\mathrm{p}(\mathbf{K})K_\mathrm{n}\mathrm{e}^{i\mathbf{K}\mathbf{r}} + (\bar{\epsilon}^0_\mathrm{ij} + \epsilon^\mathrm{A}_\mathrm{ij})r_\mathrm{j} \tag{4}$$

where $\bar{\epsilon}^0_\mathrm{ij}$ is the spatial average of the stress-free strain, $\epsilon^\mathrm{A}_\mathrm{ij}$ is related to the external stress by Hooke's law ($\sigma^\mathrm{A}_\mathrm{ij} = \lambda_\mathrm{ijkl}\epsilon^\mathrm{A}_\mathrm{kl}$), $G_{ij}(\mathbf{K})$ is the Fourier transform of Green's function (defined by $G^{-1}_\mathrm{ij}(\mathbf{K}) = \lambda_\mathrm{imjl}K_\mathrm{m}K_\mathrm{l}$) and $\sigma^{00}_\mathrm{ij}(p)$ is related to the stress-free strain $\epsilon^{00}_\mathrm{ij}(p)$ also by Hooke's law. From Eq. (4), the strain field can be computed and replaced in Eq. (2), yielding the equilibrium elastic energy:

$$E^\mathrm{el} = \frac{V}{2}\sum_{\mathbf{K}\neq 0}\sum_{p,q:phase} B_\mathrm{pq}(\mathbf{K})\theta_\mathrm{p}(\mathbf{K})\theta^*_\mathrm{q}(\mathbf{K}) - V\sum_{p:phase}\sigma^\mathrm{A}_\mathrm{ij}\epsilon^{00}_\mathrm{ij}(p)\theta_\mathrm{p}(\mathbf{K}=0) \tag{5}$$

with

$$B_\mathrm{pq}(\mathbf{K}) = \sigma^{00}_\mathrm{ij}(p)\epsilon^{00}_\mathrm{ij}(q) - K_\mathrm{i}\sigma^{00}_\mathrm{ij}(p)G_\mathrm{jm}(\mathbf{K})\sigma^{00}_\mathrm{mn}(q)K_\mathrm{n} \tag{6}$$

Matrices $B_{pq}(\mathbf{K})$ are intrinsic quantities which characterize the elastic interactions between phases p and q. The driving force on a phase p at point $\mathbf{r}$ is defined as the opposite of the functional derivative of the free energy of the system with respect to the field θ_p taken at $\mathbf{r}$:

$$F_\mathrm{p}(\mathbf{r}) = -\frac{\delta E^\mathrm{el}}{\delta\theta_\mathrm{p}(\mathbf{r})} = \sigma^\mathrm{A}_\mathrm{ij}\epsilon^{00}_\mathrm{ij}(p) - \sum_{\mathbf{K}\neq 0}\sum_{q:phase} B_\mathrm{pq}(\mathbf{K})\theta_\mathrm{q}(\mathbf{K})\mathrm{e}^{i\mathbf{K}\mathbf{r}} \tag{7}$$

This equation can be rewritten in real space by replacing B_{pq} by its expression (Eq. (6)) and identifying the gradient of displacement and the Fourier transform of the stress-free strain:

$$F_\mathrm{p}(\mathbf{r}) = (\sigma^\mathrm{el}_\mathrm{ij}(\mathbf{r}) + \sigma^\mathrm{A}_\mathrm{ij})\epsilon^{00}_\mathrm{ij}(p) \tag{8}$$

where $\sigma^\mathrm{el}_\mathrm{ij}(\mathbf{r}) = \lambda_\mathrm{ijkl}(\epsilon_\mathrm{kl}(\mathbf{r}) - \epsilon^0_\mathrm{kl}(\mathbf{r}))$ is the elastic stress. Therefore, the driving force $F_p(\mathbf{r})$ is the virtual work that would be done by the stress if the system at point $\mathbf{r}$ was transformed from the reference state into phase p.

2.2. Equivalence between dislocation loops and inclusions

The present method is based on the elastic equivalence between a dislocation loop of Burgers vector $\mathbf{b}$ and normal $\mathbf{n}$ and a platelet inclusion, bounded by the dislocation line, of vanishing thickness a and of stress-free strain:

$$\epsilon^{00}_\mathrm{ij} = \frac{1}{2}\frac{b_\mathrm{i}n_\mathrm{j} + b_\mathrm{j}n_\mathrm{i}}{a} \tag{9}$$

with a shape function $\theta(\mathbf{r}) = 1$ in the inclusion and $\theta(\mathbf{r}) = 0$ outside. We call this shape function a *dislocation field*. The method will be presented keeping a finite thickness a but note that it is implemented in the limit of vanishing thickness $a \to 0$ (the stress-free strain can then be written in terms of a delta-function defined over the loop surface: $\epsilon^0_\mathrm{ij}(\mathbf{r}) = (b_\mathrm{i}n_\mathrm{j} + b_\mathrm{j}n_\mathrm{i})\delta_\mathrm{s}(\mathbf{r})/2$). The equivalence between inclusion and dislocation loop is proved [12] by showing that both produce the same displacement field given by Burgers formula [15].

This equivalence allows us to introduce dislocations in an existing Phase Field code simply by adding extra phases made of platelet inclusions with stress-free strains given by Eq. (9). The present method inherits of the generality of classi-

cal PFM: the medium may be isotropic or anisotropic and no constraint is imposed on the shape and character of the dislocations.

In terms of plasticity, the stress-free strain given by Eq. (9), taking a as the interplanar spacing, is the plastic strain imposed along the loop surface and is equivalent to the eigenstrain introduced by Mura [10]. In that sense, the present method is equivalent to applying plastic strains along loop surfaces and is based on the same physical ground as the Discrete-Continuous model of Devincre et al. [6,16]. Note, however, that in the later case, elasticity is treated in real space by means of the Finite Element method. Moreover, the finite elements are of dimensions much larger than in the present case, requiring homogenization and localization methods [16].

2.3. Case of crystalline solids and multislip deformation

In crystalline solids, dislocations belong to a finite set of slip systems. For example, there are 12 slip systems in FCC crystals, made of $a/2\langle 110\rangle$ Burgers vectors and $\{111\}$ slip planes. In the context of the present model, configurations with several slip systems can be modeled by associating one extra phase to each slip system, since both are characterized by a Burgers vector and the normal to a plane. The local stress-free strain is then the sum of the strains due to the various slip systems and the energy is given by Eq. (5) with indices p and q running over the slip systems.

Moreover, and by way of contrast with usual phases, multiple dislocation loops can overlap or glide over the same location in space. As a consequence, the dislocation field of a system, i.e. the total plastic strain of the system, can take any positive or negative integer value, depending on the sign and number of dislocations which have glided over the point of consideration [11,12].

In the present article, for the sake of simplicity, the model will be illustrated on a simple cubic system with $\{001\}$ slip planes and $\langle 001\rangle$ Burgers vectors. Application of the model to FCC crystals will be discussed in Section 7.

Note finally that the driving force on a slip system p, obtained by replacing the dislocation stress-free strain (Eq. (9)) in Eq. (8), is simply equal to the Resolved Shear Stress (RSS) applied to the system, multiplied by a factor b/a, i.e. the component of the stress tensor which acts on dislocations to make them glide. This signification of the driving force will be used in Section 4 to apply dynamics to the dislocation fields.

3. Sub-grid dislocation cores

The computer implementation of the method presented in previous section requires a discretization of real space[1] which is usually performed on a cubic grid. In order to perform micronscale simulations, the grid spacing d must be at least of the order of a few nanometers, and thus of the order of ten Burgers vectors. In a PFM based on this single length scale, all spatial dimensions will be commensurate with it. In particular, in a Diffuse Interface approach [11,12], dislocation fields vary continuously from one integer value to another one in transition regions which represent dislocation cores. These cores have a width of typically $5d \sim 50b$ since narrower cores experience grid pinning, a numerical effect well known in the context of phase transformations: narrow interfaces in a discretized space have a low mobility.

This minimum core width of approximately $50b$ is very large compared to dislocation cores in crystalline solids which are close to b. Since the core size controls the maximum stress near dislocations ($\sigma_{\max} \sim \dfrac{\mu}{2\pi}\dfrac{b}{d_0}$ where d_0 is the core radius), large cores lead to weak singularities and therefore weak short-range interactions between dislocations and also between dislocations and concentration fields.

[1] In a discrete space, the forward Fourier transform of Eq. (3) becomes a discrete sum while the backward Fourier transform is limited to the first Brillouin zone of the grid (BZ):

$$\theta^{\mathrm{d}}(\mathbf{K}) = \frac{1}{N}\sum_{n}\theta^{\mathrm{d}}(n)\mathrm{e}^{-\mathrm{i}\mathbf{K}\mathbf{r}_{\mathrm{n}}}$$
$$\theta^{\mathrm{d}}(n) = \sum_{K\in BZ}\theta^{\mathrm{d}}(\mathbf{K})\mathrm{e}^{\mathrm{i}\mathbf{K}\mathbf{r}_{\mathrm{n}}} \tag{10}$$

As a consequence, modeling realistic dislocation cores is crucial and cannot be achieved with a PFM based on a single length scale. In this section, we present a method to introduce a second independent length scale in a PFM, associated to the dislocation core radius which allows to model dislocation cores smaller than the grid spacing.

3.1. Loopons

The dislocation fields are decomposed into a superposition of elementary loops, which we will call *loopons* [17]. The fields are supposed to be constant over the surface of the loopons and may be discontinuous between loopons.

In order to be more specific, consider a cubic crystal with ⟨001⟩{001} slip and prismatic systems. The medium is continuous but we superpose on the later a discrete cubic grid as shown in Fig. 1. Nine elementary loops (one for each system) may be associated to each grid point. Fig. 1 shows, for a given grid point n, the loopon surface associated with systems with a plane perpendicular to the Z direction. There are two other possible surfaces, perpendicular to the X and Y directions respectively. Three systems are associated to each surface (two slip systems and one prismatic system) depending on the direction of the Burgers vector. As shown in Fig. 1, the surfaces of the loopons are square surfaces, centered around the grid-points and shifted with respect to the latter by a distance $d/2$ in the direction normal to the surface. The motivation of this shift will be discussed in Section 3.3. Any dislocation field may then be decomposed into a sum of fields of loopons:

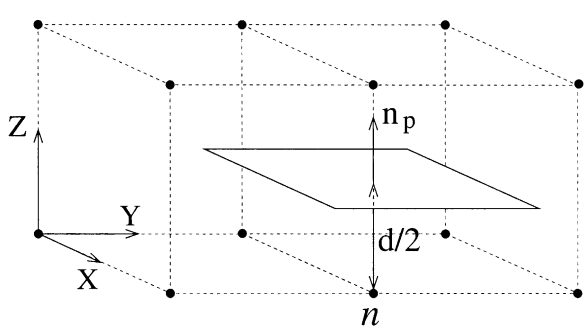

Fig. 1. Loopon associated with grid point n in a cubic grid of spacing d. The loopon is shifted with respect to the grid by $d/2$ in the direction of $\mathbf{n}_p$, the normal of the loopon system.

$$\theta_p(\mathbf{r}) = \sum_n \theta_p^d(n) S_p(\mathbf{r} - \mathbf{r}_n) \tag{11}$$

where n runs over all grid points. S_p is the shape function of the loopon of system p associated to the grid point at the origin of the grid. If (x_p, y_p, z_p) denote spatial coordinates expressed in a reference basis linked to system p (direction Z_p is the ⟨001⟩ direction parallel to the normal n_p and directions X_p and Y_p are the ⟨001⟩ directions perpendicular to n_p), S_p is written as:

$$S_p(\mathbf{r}) = H_{d/2}(x_p) H_{d/2}(y_p) H_{a/2}(z_p - d/2) \tag{12}$$

where $H_{d/2}(x) = 1$ if $|x| < d/2$ and 0 otherwise.

3.2. Decoration

In order to compute the elastic energy given in Eq. (5), the Fourier transform of the dislocation field must be computed. From Eq. (11), we have:

$$\theta_p(\mathbf{K}) = \theta_p^d(\mathbf{K}) S_p(\mathbf{K}) \tag{13}$$

where $\theta_p^d(\mathbf{K})$ is the discrete Fourier transform of $\theta_p^d(n)$ (Eq. (10)) and $S_p(\mathbf{K}) = \frac{1}{d^3}\int_V dV\, S_p(\mathbf{r}) e^{-i\mathbf{K}\mathbf{r}}$ is the Fourier transform of S_p:

$$S_p(\mathbf{K}) = \frac{a}{d} \frac{\sin(K_x^p d/2)}{K_x^p d/2} \frac{\sin(K_y^p d/2)}{K_y^p d/2} \frac{\sin(K_z^p a/2)}{K_z^p a/2} e^{-iK_z^p \frac{d}{2}} \tag{14}$$

In the limit $a \to 0$, the term $\frac{\sin(K_z^p a/2)}{K_z^p a/2}$ is equal to unity.

The elastic energy in Eq. (5) is written in a continuous medium as an infinite sum over K-vectors. However, since $\theta_p^d(\mathbf{K})$ is a discrete Fourier transform, it is periodic over the Brillouin zones of the grid. Therefore, when replacing Eq. (13) into Eq. (5), a decomposition of the K-vectors into a vector of the first Brillouin zone $\left(K_i = 2\pi \frac{n_i}{N_i d},\ -N_i/2 < n_i \le N_i/2\right)$ plus a vector of the Reciprocal Lattice

(RL) of the grid $\left(G_i = 2\pi\frac{m_i}{d}, m_i \in \mathbb{Z}\right)$ allows to factorize the discrete Fourier transforms, yielding:

$$E^{el} = \frac{V}{2}\sum_{\mathbf{K}\in BZ^{*}p,q:syst.}\sum B^{dec}_{pq}(\mathbf{K})\theta^{d}_{p}(\mathbf{K})\theta^{d*}_{p}(\mathbf{K}) \qquad (15)$$

$$-V\sum_{p:syst.}\sigma^{A}_{ij}\frac{a}{d}\epsilon^{00}_{ij}(p)\theta^{d}_{p}(\mathbf{K}=0)$$

where BZ^{*} denotes the first Brillouin zone without the origin and:

$$B^{dec}_{pq}(\mathbf{K}) \qquad (16)$$

$$= \sum_{\mathbf{G}\in RL} B_{pq}(\mathbf{K}+\mathbf{G})S_{p}(\mathbf{K}+\mathbf{G})S^{*}_{q}(\mathbf{K}+\mathbf{G})$$

Eq. (15) has the usual form of the coherency elastic energy in a discrete medium, with a summation limited to the first Brillouin zone. Interaction matrices B^{dec}_{pq} called *decorated* interaction matrices, are written as sums over the Reciprocal Lattice. Physically, they correspond to the Fourier transform of the interaction energy of a pair of loopons belonging to systems p and q. As in the classical Microelasticity theory, these matrices depend only on material parameters and stress-free strains and are independent of the fields. They may therefore be computed before any simulation and the summation in the Reciprocal Lattice represents no extra computing time during the simulation.

A similar approach has already been proposed in the case of a concentration field [14]. However, in most PF applications, one is interested in precipitates much larger than the grid spacing for which the real interface thickness does not play any particular role. In such cases, the summation over the reciprocal lattice vectors **G** in Eq. (16) may be restricted to the first Brillouin zone, leading to the usual diffuse interface modeling. In the case of dislocations, reproducing a realistic core size is crucial. As explained below, this will be done in Eq. (16) by taking into account multiple Brillouin zones and by appropriately selecting the cut-off procedure.

Upon computer implementation, the RL summation of Eq. (16) must be truncated to a given number of Brillouin zones. This number of zones sets the second length scale of the PFM since it determines the variation distance of the dislocation fields between loopons, i.e. twice the dislocation core radius. More precisely, if the summation is performed for $G_i = 2\pi\frac{m_i}{d}$ with $-N_{BZ} \le m_i \le N_{BZ}$, the dislocation core radius is approximately equal to $r_c = d/2(2N_{BZ}+1)$.

This second length scale r_c is the new length scale associated with the dislocation core radius, while the grid spacing is the scale associated with slowly varying fields, such as the long-range decay of the elastic fields.

Note finally that when decoration is accounted for, the driving force on a system p has to be defined with respect to the discrete field $\theta^{d}_{p}(n)$:

$$F_{p}(n) = -\frac{1}{d^3}\frac{\partial E^{el}}{\partial\theta^{d}_{p}(n)}$$

$$= \sigma^{A}_{ij}\frac{a}{d}\epsilon^{00}_{ij}(p) - \frac{1}{d^3}\sum_{\mathbf{K}\neq\mathbf{0}}\sum_{q:phase} B^{dec}_{qp}(\mathbf{K})\theta^{d}_{q}(\mathbf{K})e^{i\mathbf{K}\mathbf{r}_n}$$

$$= \langle\sigma^{el}_{ij}(\mathbf{r})\rangle + \sigma^{A}_{ij})^{p}_{n}\frac{b_i(p)n_j(p)}{d} \qquad (17)$$

where $\langle\sigma\rangle^{p}_{n}$ is the average value of σ on the surface of the loopon of system p associated to grid-point n: $\langle\sigma\rangle^{p}_{n} = \frac{1}{d^2}\int_{S^{p}_{n}} dS\,\sigma(\mathbf{r})$ in the limit of vanishing thickness a. The driving force on a loopon is therefore the Resolved Shear Stress applied to the system of the loopon and averaged over its surface.

3.3. Test of the decoration technique

In this section, we investigate how the dislocation stress field is influenced by: (1) the decoration of the interaction matrices; and (2) the shift of the loopons with respect to the grid. More precisely, instead of the stress, we consider the driving force on the dislocation systems given by Eq. (17), i.e. the RSS averaged over the loopon surfaces. We perform 2D simulations in a 128×128 square grid with spacing $d = 10b \sim 3$ nm. Isotropic elasticity is used with: $C_{11} = 170$, $C_{12} = 70$, $C_{44} = 50$ in units of 10^9 Pa. Dislocation cores of the order of b are modeled by using a decoration based on

5×5 Brillouin zones ($N_{BZ} = 2$ with the notations of previous section).

As shown schematically in Fig. 2 (in the simulations, the loops have a width of 48 d), we consider two loops of same Burgers vector perpendicular to the plane of the figure. The loops join along their line of intersection such that, in a continuous medium, they produce only two screw dislocations, the two other dislocations annihilating each other along the line of junction. The loops are shifted with respect to the grid in the direction of their normal and lie at mid-distance between grid planes. We discuss first the necessity of this shift to reproduce annihilation between dislocations.

Fig. 3 focuses on the junction region with and without shifting the loops with respect to the grid. Fig. 4(a) shows the driving force on the system of the horizontal loop along the dashed line of Fig. 2, i.e. the YZ component of the stress tensor averaged over the surface of the loopons of the system.

Fig. 3(a) shows that without shift, the loops cannot join along a same line and therefore, cannot annihilate exactly. As a consequence, the RSS in Fig. 4(a) is peaked at the position of the supposed

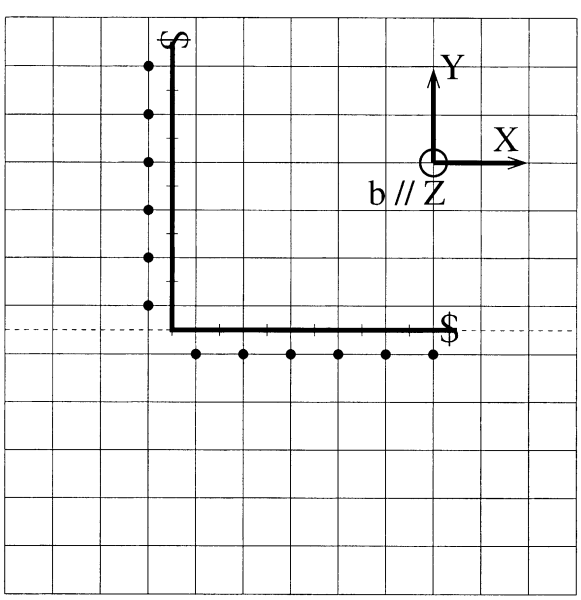

Fig. 2. 2D configuration consisting of two loops infinite in the Z direction. The loops end on screw dislocations noted by the $ signs. Grid points associated with a dislocation field equal to 1 are highlighted.

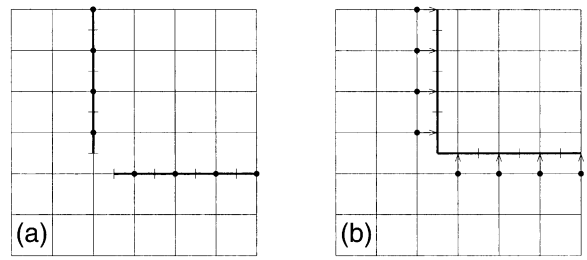

Fig. 3. Annihilation region between loops (a) without and (b) with shifting the loops with respect to the grid. The arrows in (b) link the grid points to their corresponding loopon.

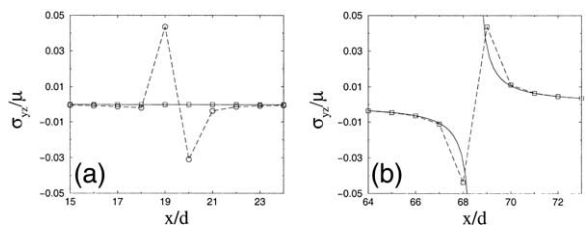

Fig. 4. Stress field along the dashed line of Figure 2, (a) in the annihilation region and (b) near the core of the dislocation contained in this line. Circles and squares correspond to simulations respectively without and with shifting the loops. The solid line in (b) is the continuum elastic prediction; the dashed lines is guides for the eye.

annihilation. On the other hand, Fig. 3(b) shows that, thanks to the shift, the loops may join along a same line, removing the peak in the stress field. The shift is therefore crucial to reproduce annihilation between dislocations.

Fig. 4(b) compares, in the region of the dislocation contained in the dashed line of Fig. 2, the simulated RSS and the continuum elastic solution for a screw dislocation, accounting for its first-neighbor periodic images. The simulated RSS matches the continuous solution except for the loopons nearest to the dislocation line. The reason is that, the RSS being averaged over the loopon surfaces, it accounts for the divergence of the stress up to the dislocation core. Note, however, that if the stress at the center of the loopons is computed from the present model, the latter matches perfectly the elastic solution, even for the loopons nearest to the dislocation.

4. Dynamical model

We now consider a dynamical algorithm for the dislocation fields. As noted in Section 3, the usual Diffuse Interface approach cannot be used since it leads to very wide dislocation cores. We have thus developed a *discrete* algorithm where the dislocation fields $\theta_p^d(n)$ vary discretely from one integer to another one. Consequently, dislocation loops evolve discretely by addition or removal of loopons along the border of their surface.

This algorithm is formulated in terms of rate equations for the fields and is physically based on the motion of the dislocation segments that border the loops. It uses the fact that the driving force on a system is the RSS on that system, which includes the self-stress of the dislocations, as seen in previous section. The basic idea of the algorithm is therefore: (1) to locate dislocation segments (border of dislocation loops) and compute their Burgers vector; (2) to compute the RSS *applied* to the dislocation segments (i.e. remove the self-stress of the dislocations); and (3) to displace the segments proportionally to this applied RSS, as in classical DDD [6]. These three steps are now presented.

4.1. Burgers vector of a dislocation segment

In the cubic system with {001} slip planes and ⟨001⟩ Burgers vectors, the square loopons are bordered by four dislocation segments as illustrated in Fig. 5. To compute the Burgers vector b^s associated with one of these segments, we have to take into account all the loopons sharing this segment. In the case of a cubic lattice, each segment belongs to $Z = 4$ different loopons. Then b^s is simply the sum of the Burgers vectors of the Z loopons,

$$b^s = \sum_{\alpha=1}^{Z} \theta_\alpha^d b_\alpha \tag{18}$$

where θ_α^d is the value of the field of loopon α and b_α is the Burgers vector of the system of that loopon. Note that the sign of the Burgers vector b_α has to be consistent with the orientation chosen for the segment.

The computation of b^s from Eq. (18) is a convenient way to locate dislocation lines. Indeed, $b^s = 0$ corresponds to no dislocation while $b^s \neq 0$ corresponds to a dislocation segment with a Burgers vector b^s. This algorithm correctly locates the dislocation lines even in the case of non-planar loops such as the one shown in Fig. 2 where a zero Burgers vector is found along the line of junction between planar loops.

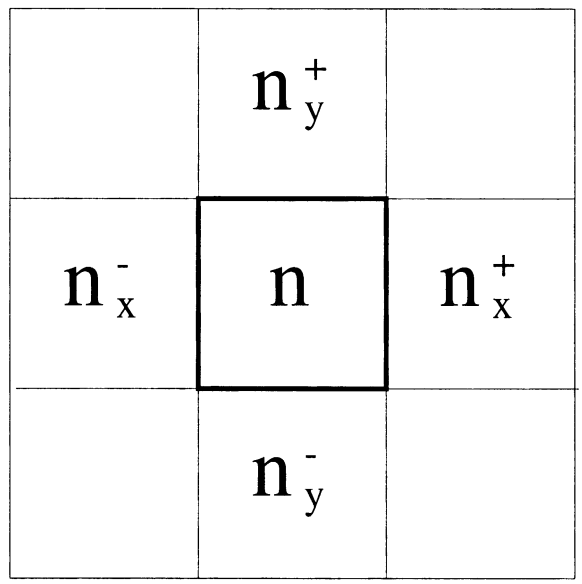

Fig. 5. Schematic representation of a loopon n bordered by four dislocation segments appearing as thick segments. These dislocations link the loopon to its four neighboring loopons $n_{x^+}, n_{x^-}, n_{y^+}, n_{y^-}$.

4.2. Dynamical equations

The algorithm is formulated in terms of rate equations for the dislocation fields $\theta_p^d(n)$. The field of a loopon such as the one shown in Fig. 5 will vary if: (1) there are dislocations on its border, i.e. at least one segment has a Burgers vector b^s different from zero; and (2) the dislocation segments move inside the loopon. The RSS *applied* to a dislocation segment lying between two loopons n and n', assuming slow variations with respect to the grid, is:

$$F_{n,n'}^A = \frac{1}{2}(F_p(n) + F_p(n')) \tag{19}$$

where $F_p(n)$ is the driving force on loopon n given by Eq. (17). The velocity of the segment is then written as $v = MdF^{A}_{n,n'}$, using the usual definition of the dislocation mobility M ($v = M\sigma b$).

In order to account for the motion of the four possible dislocation segments bordering a given loopon, we use the following expression:

$$\frac{\partial \theta_p(n)}{\partial t} = M\sqrt{((F^{+}_{x} + F^{-}_{x})^2 + (F^{+}_{y} + F^{-}_{y})^2)} \qquad (20)$$

where $(F^{+}_{x}, F^{-}_{x}, F^{+}_{y}, F^{-}_{y})$ are defined as:

$$F^{+}_{x} = F^{A}_{n,n^{+}_{x}} \times H(b^{s}_{n,n^{+}_{x}} F^{A}_{n,n^{+}_{x}}) \qquad (21)$$

$b^{s}_{n,n_x^{+}}$ is the Burgers vector of the segment common to loopons n and n_x^{+}, and H is the Heavyside function: $H(x) = 1$ if $x > 0$ and 0 otherwise.

The term in the Heavyside function ensures that there is a dislocation between the two loopons considered (otherwise the Burgers vector is 0) and that the dislocation segment glides in the direction of the loopon (otherwise the term in the Heavyside function is negative). The dynamics is made discrete by updating the dislocation fields only when the cumulated variation of a field reaches an integer value (+1 or −1).

The quadratic summation in Eq. (20) ensures that the global velocity of a straight dislocation oriented with respect to the cubic axis in ⟨100⟩ and ⟨110⟩ directions is exactly $v = M\sigma b$. In the case of a straight dislocation oriented in a ⟨1*N*0⟩ direction, we have shown analytically that the error on the dislocation velocity is less than 8%. Moreover, as will be seen in the next subsection, the anisotropy introduced by Eq. (20) in the case of a curved dislocation is small. Improving this kinetic relation would require the computation of the local curvature of the dislocations.

4.3. Tests of the dynamical model

The first test to be performed is to check that the activation stress of a Frank–Read source obtained with the present method agrees with the predictions based on continuum elasticity (see Ref. [15]). We use a 64^3 cell with a decoration based on 5^3 Brillouin zones and the same isotropic elastic coefficients as in Section 3.3. Edge sources are introduced in a configuration similar to Fig. 2 but using edge dislocations. Fig. 6 compares the activation stress obtained from the simulation to the continuum elastic prediction and shows that, for the range of source lengths considered here, both are in very good agreement.

The dynamical algorithm presented above ensures that a loop gliding because of a homogeneous stress moves with an isotropic velocity. A more crucial test is that of the evolution of a loop due its self-stress. In order to do so, we perform 3D simulations in a 128^3 grid, initially introducing a circular shear loop. We again use isotropic elastic with a decoration based on 5^3 Brillouin zones.

Fig. 7 shows the loop while shrinking. As expected from the difference in line energy between screw and edge segments, the loop adopts an ellipsoidal shape, elongated in the edge direction. The sharp angles visible on the figure at about 45 degrees from the loop Burgers vector are due to the small anisotropy introduced by the dynamical relation discussed in previous section.

A continuous elastic model is built by assuming that the loop remains circular, of radius $R = \sqrt{S/\pi}$ (we have checked in the unphysical case of an interstitial loop, which remains circular while shrinking, that the effect discussed below remains

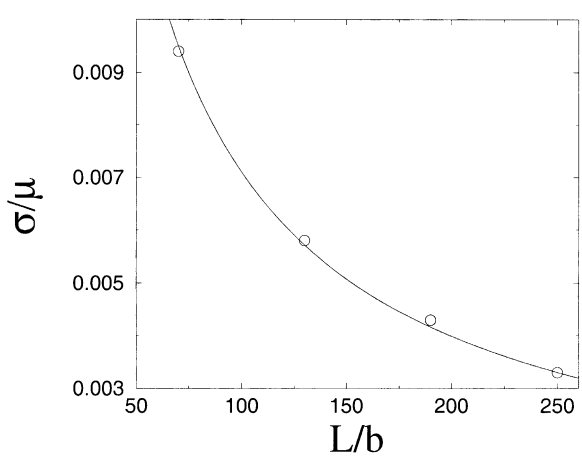

Fig. 6. Activation stress of an edge Frank–Read source as a function of its length L. Circles are the simulation results while the solid curve is the continuum elastic prediction: $\frac{\sigma}{\mu} = \frac{1-3/2\nu}{2\pi(1-\nu)}\frac{b}{L}\left(\ln\left(\frac{L}{b}\right) + 1\right)$ [15].

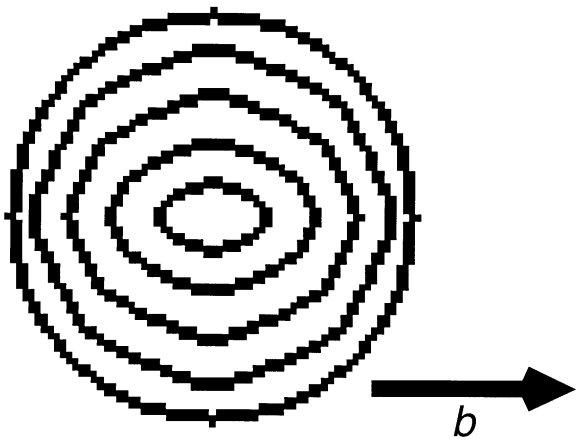

Fig. 7. Shear loop at different times while shrinking under the action of its self-stress. The two loopons neighboring each dislocation segments on the border of the loop are shown as black squares. The Burgers vector of the loop is also shown.

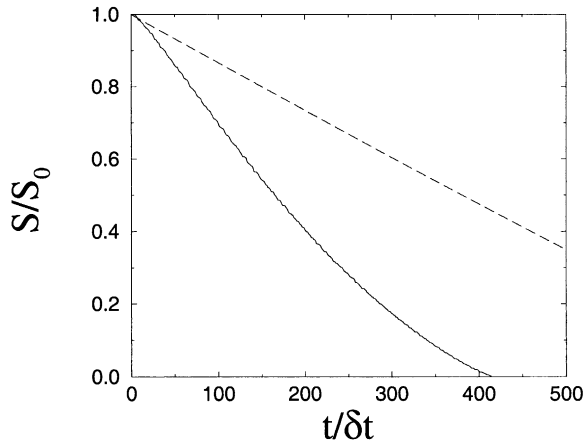

Fig. 8. Surface of a shrinking shear loop as a function of time. The surface is normalized by its initial value; time is normalized by the time step $\delta t = 100/M\mu$. Full and dashed lines are respectively the simulation results and elastic model (Eq. (22)).

true). The energy of a circular shear loop in a continuous medium $W(R)$ is given for example in Ref. [15]. Assuming that the velocity of the loop is proportional to its self-stress, the following equation is obtained:

$$\frac{dS}{dt} = -M\frac{dW}{dR} = -M\frac{2-\nu}{2(1-\nu)}\frac{\mu b^2}{4\pi}\left(\ln\left(\frac{4R}{b}\right)-1\right) \tag{22}$$

As shown in Fig. 8, the dynamical algorithm predicts shrinking velocities about three times larger than continuum elasticity. The reason for this difference is certainly linked to the edge-screw discretization of the dislocation line. In this approximation, neighboring edge and screw segments interact more strongly than they would in a smoother description of the dislocation line.

In conclusion, the dynamical algorithm proposed here leads to the correct static equilibrium states (since the Frank–Read activation stress is correctly reproduced) but overestimates, for the part due to the self-stress of the dislocations, the speed at which these states are reached.

5. Coupling with a concentration field

The main advantage of the present method is its ability to couple elastically, in a straightforward way, dislocation fields with other fields, i.e. concentration and order parameter fields. In the present article, we will focus on the case of a concentration field, keeping in mind that the generalization to order parameters is straightforward. The concentration field is modeled by means of a classical Time-Dependent Ginzburg-Landau (TDGL) model [4]. However, since the stress field produced by an edge dislocation varies from compression to tension over a distance of the order of the dislocation core radius, the concentration field is expected to vary abruptly in this region. Therefore, variation distances smaller than the grid spacing must also be allowed for the concentration field. This is accomplished by applying to the concentration field the decoration technique developed for dislocations.

For a coherent phase-separating alloy with a lattice parameter mismatch between two atomic species, the chemical free energy may be represented by a Ginzburg–Landau free energy:

$$F^{\text{chem}} = \int_V dV\left(-\frac{\mu}{2}\phi^2 + \frac{\gamma}{4}\phi^4 + \frac{\lambda}{2}|\nabla\phi|^2\right) \tag{23}$$

with $c(\mathbf{r})$ being the concentration and $\phi(\mathbf{r}) = 2c(\mathbf{r})-1$.

The stress-free strain is related to the lattice mismatch by means of Vegard's law:

$$\epsilon^0_{ij}(\mathbf{r}) = \epsilon_0 \delta_{ij} c(\mathbf{r}); \quad \epsilon_0 = \frac{1}{a}\frac{\partial a}{\partial c} \tag{24}$$

Coupling with dislocation fields arises from the assumption that the local stress-free strain is the sum of the strains due to the dislocations and to the concentration field:

$$\epsilon^0_{ij}(\mathbf{r}) = \epsilon_0 \delta_{ij} c(\mathbf{r}) + \sum_{p:syst.} \epsilon^0_{ij}(p)\theta_p(\mathbf{r}) \tag{25}$$

The concentration field is assumed to be constant inside elementary cubes centered around each grid point and discontinuous between elementary cubes:

$$c(\mathbf{r}) = \sum_n c^d(n) S(\mathbf{r} - \mathbf{r}_n) \tag{26}$$

where $S(\mathbf{r})$ is the shape function of the elementary cube at the origin of the grid: $S(\mathbf{r})=H_{d/2}(x)H_{d/2}(y)H_{d/2}(z)$, with the notations of Eq. (12).

As in the case of dislocations, using the periodicity of the discrete Fourier transforms of $c^d(n)$, the elastic energy of the system may be written as a sum in Fourier space limited to the first Brillouin zone of the grid. As a result, we obtain an energy of the same form as Eq. (15) with indices p and q running over the dislocation and concentration fields. The decorated interaction matrices are as in Eq. (16) except that, when the concentration is involved, the corresponding shape function is:

$$S(\mathbf{K}) = \frac{\sin(K_x d/2)}{K_x d/2}\frac{\sin(K_y d/2)}{K_y d/2}\frac{\sin(K_z d/2)}{K_z d/2}.$$

Dynamics is applied to the concentration field by means of a Cahn–Hilliard kinetic equation:

$$\frac{\partial c(\mathbf{r})}{\partial t} = \nabla M \times c(\mathbf{r})(1-c(\mathbf{r}))\nabla \frac{\delta}{\delta c(\mathbf{r})}\{F^{chem} + E^{el}\} \tag{27}$$

where the elastic driving forces have the same form as in Eq. (17).

The decorated interaction matrices B^{dec}_{cc} differ from the interaction matrices B_{cc} used in classical Phase Field simulations. As shown in Fig. 9 which compares these matrices, they differ only for K-vectors of norm typically larger than $\pi/3d$, i.e. for fields varying rapidly, over distances less than about three grid spacings. In simulations, in order to avoid numerical grid-pinning effects, the stiffness constant λ of Eq. (23) is chosen such that interfaces between precipitate and matrix spread over typically five grid spacing, i.e. the non-zero components of the Fourier transform of the concentration field have a norm smaller than $\pi/5d$. They therefore remain in the region of reciprocal space where decorated and non-decorated interaction matrices are identical. Hence, in absence of dislocations, the decoration procedure proposed here does not influence microstructural evolution, as we have checked directly on simulations. On the other hand, in presence of dislocations, the concentration field varies near dislocation lines over distances close to the Burgers vector and large K-vectors are visited. In this case, decoration of the interaction matrices is required to describe properly the strain-induced interactions.

6. Application to alloy hardening

We present an example of simulation of a dislocation loop gliding in a microstructure made of platelet inclusions separated by channels. This micro-

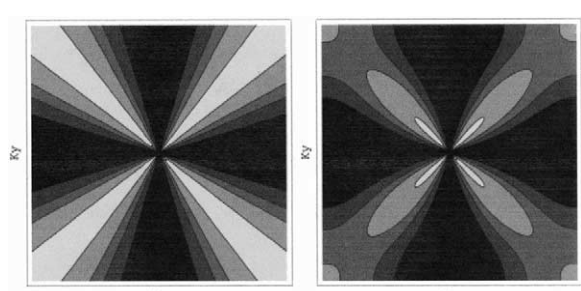

Fig. 9. Comparison of decorated (right) and non-decorated (left) interaction matrices in the central (001) plane of the first Brillouin zones of reciprocal space. Decoration is based on 5^3 Brillouin zones in a 128^3 cubic grid. The values goes from 3 to 6 $C_{44}\frac{b}{d}\epsilon_0$ when the grayscale varies from black to white.

structure is representative of a late-stage γ/γ' structure and has been considered recently in [6].

We consider a binary alloy with a lattice mismatch of 1.4%. Anisotropic elasticity is used with: $C_{11} = 102$, $C_{12} = 70$, $C_{44} = 50$ in units of 10^9 Pa. The parameters of Eq. (23) are: $\lambda/d^2C_{44} = \mu/C_{44} = \gamma/C_{44} = 3.4 \times 10^{-4}$. An interfacial energy $\gamma_s = 50$ mJ.m^{-2} is reproduced by setting the grid spacing $d = 3$ nm. Concerning the dislocations, in order to model cores of the order of b with $d \sim 10b$, decoration is applied to both dislocation and concentration fields using 5^3 Brillouin zones in a cubic 128^3 simulation cell. The cell is oriented such that the horizontal Z planes are (111) planes while the X direction of the cell is aligned in the $[1\bar{1}0]$ direction of the cubic axis.

The microstructure obtained in absence of dislocations is shown in Fig. 10. It consists of platelet inclusions with facets perpendicular to the $\langle 001 \rangle$ directions. As seen in Fig. 10(a), these inclusions leave in (111) planes traces parallel to the three $\langle 110 \rangle$ directions of these planes. As shown in the figure, these directions are called A, B and C and correspond to the $[1\bar{1}0]$,$[01\bar{1}]$ and $[\bar{1}01]$ directions respectively. Precipitates and channels will be referred by their orientation using this convention.

As shown in Fig. 10(a), a circular shear loop is initially placed in a channel of type A. The Burgers vector of the loop is the $[\bar{1}01]$ vector parallel to direction C. Our aim is to investigate the behavior of this loop in the microstructure. The presence of the latter is revealed through the Resolved Shear Stress it produces in the glide plane of the loop, shown in Fig. 10(b). As seen in this figure, the RSS is positive in channels of type A and tends to open the shear loop and is negative in the precipitates. The interface between channels and inclusions of type A are therefore stable equilibrium positions for the dislocation. The situation is reversed in channels of type B where the RSS is negative in the channels and positive in the inclusions. The RSS in channels of type B therefore tends to close the loop. Finally, the RSS is close to 0 both in channels and inclusions of type C. The dependence of the RSS on the orientation of the channels can be understood from the fact that if the loop considered here expands in a channel of type A it leaves interface dislocations between channel and inclusion with a Burgers vector which decreases the lattice parameter mismatch between the channel and the inclusion. Expansion in channels of type A is therefore favorable. Inversely, the interface dislocations left by the dislocation considered here in channels of type B increase the lattice parameter mismatch and are therefore unfavorable. Finally, the interface dislocations left in channels of type C would be of screw character and would therefore not change the lattice parameter difference. The loop therefore does not interact with channels of type C.

The behavior of the dislocation under an applied RSS of $2.45 \times 10^{-3}C_{44}$ is shown in Fig. 11. This stress is above the activation stress of the loop but below the interface stress. The dislocation there-

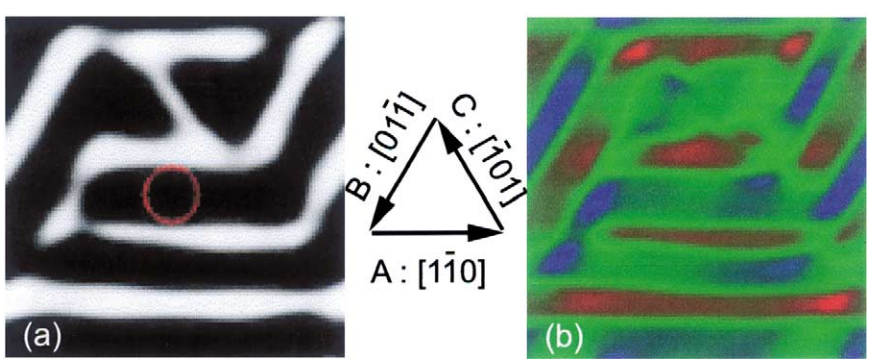

Fig. 10. Late-stage γ/γ' structure: (a) microstructure with a loop of Burgers vector in the C $[\bar{1}01]$ direction, (b) RSS due to the microstructure in the plane of the loop. The RSS varies from $-6 \times 10^{-3}C_{44}$ to $6 \times 10^{-3}C_{44}$ when the color varies from blue to red; green corresponds to zero RSS.

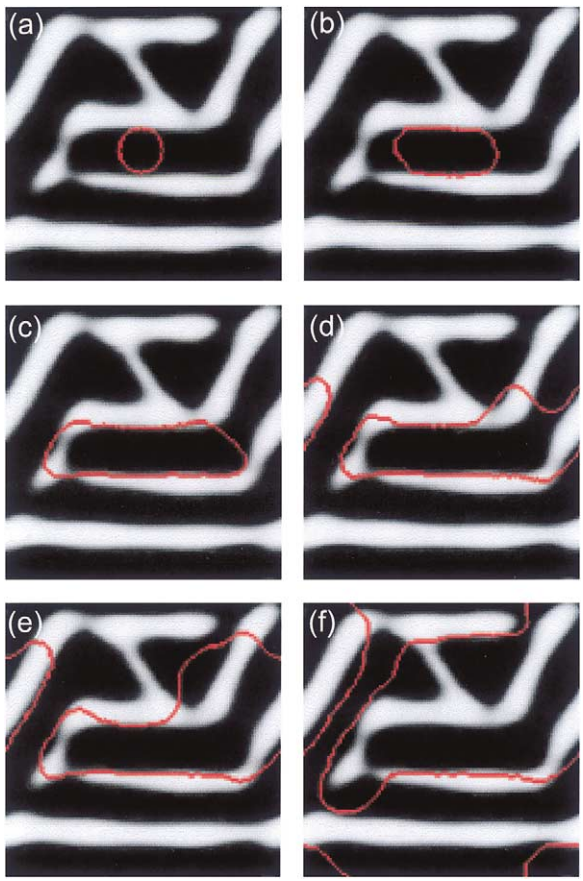

Fig. 11. Loop expansion under the action of a RSS of $2.45 \times 10^{-3} C_{44}$.

fore expands in the channel, leaving dislocation segments along the interface between channel and inclusion. When the loop reaches the end of the channel on the right-hand side, it is attracted by the B precipitates and repelled by the channel [see Fig. 10(b)]. As a consequence and as seen in the figure, the dislocation propagates in the precipitates and, by a line tension effect, is pulled through the channel. On the left-hand side, the dislocation is stopped at the interface of type B. Finally, the long arm of the dislocation on the right-hand side detaches from the B precipitates and glides through the microstructure.

More simulations would be required to investigate in details the behavior of dislocation loops in a complex microstructure such as the one considered here. The aim of this section was only to illustrate the capabilities of the method, while detailed studies will be addressed in a future article.

7. Conclusion

We have presented a Phase Field method to study, at the micronscale, the mutual interactions between dislocations and precipitation microstructures. The main advantages of the method are: (1) its ability to couple elastically dislocations to any other field, such as a concentration field; and (2) its straigthforward treatment of boundary conditions (periodic conditions but also flat free-surfaces).

Special attention has been paid to the treatment of dislocation cores, which radius must be of the order of the lattice parameter in order to have a realistic short-range description of dislocations. The method proposed here contains two length scales, which reflect the inherently multiscale nature of dislocations which requires a correct treatment of both short- and long-range interactions. By way of contrast, the behavior of precipitates does not depend strongly on the width of their interface and Diffuse Interface approaches may be used in this case whereas it cannot be used for dislocations. The decoration technique presented here allows to account for multiple Brillouin zones with unknowns only in the first Brillouin zone (the discrete Fourier transform of the fields). Moreover, since in the presence of dislocations, the concentration field is expected to vary over distances of the order of the dislocation core radius, the decoration had to be extended to the concentration field as well.

Application of the present *decorated* Phase Field method to FCC multislip systems is straightforward. The basic ingredient, i.e. the thin loopons, will be equilateral triangles with {111} surfaces and edges along the three ⟨110⟩ directions contained in the surface. Real space will still be discretized over a cubic grid, with four loopon surfaces associated to each grid point, forming an equilateral tetrahedron centered at the grid point. Twelve loopons (one for each slip systems) will thus be associated to each grid point. Therefore, as in the simple case illustrated here of a cubic system, the topology required to treat correctly local

core interactions will be included in the model. In particular, loops on cross-slip systems, i.e. sharing a given ⟨110⟩ direction, will be able to form junctions along this direction since the loopons of both systems will have edges along this direction. By recourse to the decoration technique, both short- and long-range properties of dislocations will be reproduced, opening the way to the study of plasticity in FCC alloys in multislip conditions.

References

[1] Cottrell AH. In: Mott NF, editor. Report of a conference on strength of solids. London: The Physical Society; 1948, p. 30.
[2] Larché FC. In: Nabarro FRN, editor. Dislocations in solids, 4. Amsterdam: North-Holland; 1979, p. 135.
[3] Gerold V. In: Nabarro FRN, editor. Dislocations in solids, 4. Amsterdam: North-Holland; 1979, p. 219.
[4] Phase transformations and evolution in materials. In: The Minerals, Metals and Materials Society, Turchi EA, Gonis A (Eds.), Warrendale, Pennsylvania, 2000.
[5] Fratzl P, Penrose O, Lebowitz JL. J Stat Phys 1999;95:1429.
[6] Devincre B, Kubin LK, Lemarchand C, Madec R. Mat Sci Eng A 2001;211:309–10.
[7] Bulatov VV, Tang M, Zbib HM. MRS Bulletin 2001;26.
[8] Léonard F, Desai RC. Phys Rev B 1998;58:8277.
[9] Hu SY, Chen LQ. Acta Mater 2001;49:463.
[10] Mura T. Micromechanics of defects in solids. Dordrecht: Kluwer Academic Publisher, 1982.
[11] Wang YU, Jin YM, Cuitiño AM, Khachaturyan AG. Acta Mater 2001;49:1847.
[12] Rodney D, Finel A. MRS Symp Proc 2001;652:Y4.9.1–Y4.9.6.
[13] Nabarro FRN. Phil Mag 1951;42:1224.
[14] Khachaturyan AG. Theory of structural transformation in solids. New York: Wiley, 1983.
[15] Hirth JP, Lothe J. Theory of dislocations. Malabar: Krieger, 1992.
[16] Lemarchand C, Devincre B, Kubin LP, Chaboche JL. J Mech Phys Solids 2001;49:1969, 1982.
[17] Shenoy VB, Ortiz M, Phillips R. Modeling Simul Mater Sci Eng 1999;7:603.